Three-dimensional lattice Boltzmann model for gaseous flow in rectangular microducts and microscale porous media

G. H. Tang,[a] W. Q. Tao, and Y. L. He
State Key Laboratory of Multiphase Flow in Power Engineering, School of Energy and Power Engineering, Xi'an Jiaotong University, Xi'an 710049, China

(Received 1 November 2004; accepted 10 March 2005; published online 12 May 2005)

Microscale fluid dynamics has received intensive interest due to the rapid advances in microelectromechanical systems. In this work, the lattice Boltzmann method is applied to simulate isothermal gaseous slip flow in three-dimensional (3D) rectangular microducts and microscale porous structures. The flow characteristics in 3D microducts—including velocity profile, nonlinear pressure distribution, friction factor, and mass flow rate—are compared with analytical solutions, and the agreement is good. The flow-rate results show that due to the slip-velocity emergence at the walls, the lateral wall influence on the flow rate in 3D rectangular microducts is decreased. The predicted transport characteristics in 3D microscale porous media show that the rarefaction influence increases the gas permeability. The Klinkenberg effect is confirmed and the predicted gas permeability is qualitatively consistent with the experimental results. Furthermore, the nonlinear behavior of the porous flow at relatively higher Reynolds number is also observed. This study demonstrates that the lattice Boltzmann method can be employed to efficiently predict transport characteristics in microducts and microscale porous media. © *2005 American Institute of Physics*. [DOI: 10.1063/1.1901839]

I. INTRODUCTION

In the last decade, microelectromechanical systems (MEMS) are finding increasing applications in a variety of industrial fields.[1] However, the rapid progress in fabricating and utilizing MEMS has not been matched by the corresponding advances in our understanding of the physics involved in the operation and manufacture of small devices. Available experimental and numerical results indicate that thermal and hydraulic performances of microsized channels differ from those of macrochannels, and the measured results from different authors are often contradictory. The measured friction factors in Refs. 2–4 are significantly higher than those predicted by the continuum flow theory, while the friction factors measured in Refs. 5–7 are lower than the conventional ones.

The continuum approach will break down for large mean-free paths, as what occurs in rarefied gas dynamics. The Knudsen number, which is defined as $\mathrm{Kn}=\lambda/H$, provides a direct means of validating the continuum approach as it compares the mean-free path λ to the characteristic length H. For $\mathrm{Kn}>10$ the system can be considered as a free molecular flow. A flow is considered as a continuum for $\mathrm{Kn}<0.001$. The intermediate values of $0.1<\mathrm{Kn}<10$ are associated with a transition flow regime, while those within the range of $0.001<\mathrm{Kn}<0.1$ are representative of a slip flow regime. The Navier–Stokes equation and the energy equation may be applied to flows within the slip regime or those that are marginally transitional if the first-order or second-order velocity slip and temperature-jump boundary conditions are employed at the solid walls. Analytical solutions or numerical simulations of fluid flow and heat transfer in microchannels were conducted by solving the Navier–Stokes equation with slip boundary conditions in Refs. 8–11.

For the case of a Knudsen number larger than 0.1, in which slip flow approximation is not valid, the particle methods based on molecular dynamics (MD)[12] and the direct simulation Monte Carlo (DSMC)[13] are often used to investigate low-pressure rarefied gas flow characteristics. But there are some disadvantages in applying the MD or DSMC method to gas microflows, such as the large statistical noise and the long time it takes to reach steady states for low-speed gas flows often encountered in MEMS. The extensive number of molecules in the MD or DSMC method is another disadvantage, which makes the simulation go easily beyond the capabilities of most computers. Numerical simulations based on the linear Boltzmann equation[14,15] are suitable for solving the low-speed rarefied gas flows in the whole flow regime. But most obtained solutions are limited to simple geometries due to the complexity in performing the numerical solution of the full Boltzmann equation.

The lattice Boltzmann method (LBM) is a discrete approach that can use parallel computers conveniently to study various problems, especially for complicated boundaries such as porous media flow.[16] In traditional computational fluid dynamics, the given macroscopic equation is solved by some specific numerical discretization. While in full molecular dynamic descriptions, each individual particle is closely and accurately followed. Unlike these traditional numerical schemes, the lattice Boltzmann method solves a simplified Boltzmann equation for distributed function on a regular lattice. The macroscopic parameters are then obtained through an ensemble average of the distribution function. The lattice method can be described as a mesoscopic model that occu-

[a]FAX: 011-86-29-8266-9106; electronic mail: ghtang@mail.xjtu.edu.cn

pies a position between the full molecular dynamics and macroscopic descriptions by means of differential equations. Therefore, it is much more computationally efficient than the MD or DSMC method. The LBM has been shown to be a very efficient tool for flow simulation in highly complex geometries and has achieved considerable success in simulating flows and associated transport phenomena in porous media.[17] In fact, the lattice-gas automata method, the ancestor of the LBM, was already applied to study the flows in porous media in the early 1980s;[18,19] the reliability and efficacy of the LBM in simulating flows in 2D and 3D geometries[20–26] were confirmed soon after its emergence in 1988.[27]

In the complicated geometry flow, such as the gas fuel transport through carbon paper in fuel cells or the nanopore flows,[28] the mean-free path of the gas molecules may be comparative with the pore size; so the slip effect must be involved the gaseous flow through such structures. However, the conventional numerical methods such as the finite difference or the DSMC is inefficient due to the highly complicated boundary conditions. Thus, it is quite evident and necessary to extend the lattice Boltzmann method to simulate the flow in the slip or transition regime.

In this paper, we present a three-dimensional (3D) lattice Boltzmann model for simulating isothermal gaseous flow in rectangular microducts. This 3D model is an extension of the two-dimensional model in our previous work.[29] The article is organized into the following sections: The lattice Boltzmann methodology and the present 3D lattice Bhatnagar–Gross–Krook (LBGK) model are introduced in Sec. I. In Sec. II, we present typical results and compare these with analytical and experimental data. In Sec. III, we apply the present LBM model in a 3D microscale porous structure. Sec. IV concludes the paper.

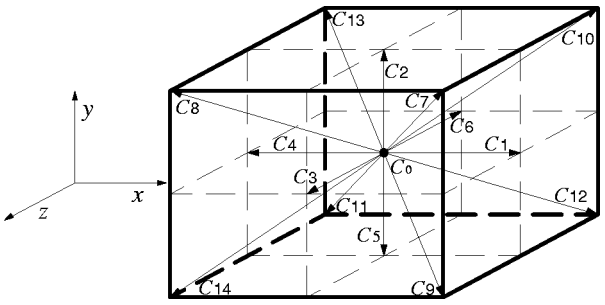

FIG. 1. A sketch of the D3Q15 model.

II. THREE-DIMENSIONAL LATTICE BOLTZMANN BGK MODEL FOR MICROFLOWS

In the lattice Boltzmann method, the particle distribution function $f_i(\mathbf{r},t)$ at point $\mathbf{r}$ and time t satisfies the following lattice Boltzmann equation with BGK collision operator written in physical units:[30,31]

$$f_i(\mathbf{r}+\mathbf{c}_i\Delta t, t+\Delta t) = f_i(\mathbf{r},t) - \frac{1}{\tau}[f_i(\mathbf{r},t) - f_i^{\mathrm{eq}}(\mathbf{r},t)], \tag{1}$$

where f_i^{eq} is the local-equilibrium distribution function and τ is the dimensionless single relaxation time which fixes the rate of approach to equilibrium. The parameter $\mathbf{c}_i$ is the particle discrete velocity. In the study of 3D flow problems, the 3D 15-bit discrete velocity model (D3Q15), shown in Fig. 1, is usually used. The velocity vectors of the particle of this model are given in

$$[\mathbf{c}_1,\mathbf{c}_2,\mathbf{c}_3,\mathbf{c}_4,\mathbf{c}_5,\mathbf{c}_6,\mathbf{c}_7,\mathbf{c}_8,\mathbf{c}_9,\mathbf{c}_{10},\mathbf{c}_{11},\mathbf{c}_{12},\mathbf{c}_{13},\mathbf{c}_{14},\mathbf{c}_0] = \begin{bmatrix} 1 & 0 & 0 & -1 & 0 & 0 & 1 & -1 & 1 & 1 & -1 & 1 & -1 & -1 & 0 \\ 0 & 1 & 0 & 0 & -1 & 0 & 1 & 1 & -1 & 1 & -1 & -1 & 1 & -1 & 0 \\ 0 & 0 & 1 & 0 & 0 & -1 & 1 & 1 & 1 & -1 & -1 & -1 & -1 & 1 & 0 \end{bmatrix} c, \tag{2}$$

where c is the particle-streaming speed, $c=\sqrt{3RT_0}$, R is the specific gas constant and T_0 is the reference gas temperature.

One of the equilibrium distribution functions of this 3D model is give by Qian *et al.*[31]

$$f_i^{\mathrm{eq}} = \rho\omega_i\left[1 + \frac{3}{c^2}(\mathbf{c}_i\cdot\mathbf{u}) + \frac{9}{2c^4}(\mathbf{c}_i\cdot\mathbf{u})^2 - \frac{3}{2c^2}\mathbf{u}^2\right], \tag{3}$$

where w_i is the weighting coefficient and is $2/9$ for $i=0$, $1/9$ for $i=1,2,3,4,5,6$, and $1/72$ for $i=7,8,9,10,11,12,13,14$. The mass density is $\rho=\sum_i f_i$ and the momentum density is $\rho\mathbf{u}=\sum_i f_i\mathbf{c}_i$. The pressure and kinematic viscosity are given in

$$p = \frac{\rho c^2}{3}, \quad v = \frac{c^2\Delta t}{6}(2\tau - 1) \tag{4}$$

Grunau[32] also presented an equilibrium distribution function for the D3Q15 LBGK model in the following equation

$$f_0^{\mathrm{eq}} = \rho\left(\frac{1}{8} - \frac{1}{3c^2}\mathbf{u}^2\right),$$

$$f_{1,\ldots,6}^{\mathrm{eq}} = \rho\left(\frac{1}{8} + \frac{1}{3c^2}(\mathbf{c}_i\cdot\mathbf{u}) + \frac{1}{2c^4}(\mathbf{c}_i\cdot\mathbf{u})^2 - \frac{1}{6c^2}\mathbf{u}^2\right),$$

$$f_{7,\ldots,14}^{\mathrm{eq}} = \rho\left(\frac{1}{64} + \frac{1}{24c^2}(\mathbf{c}_i\cdot\mathbf{u}) + \frac{1}{16c^4}(\mathbf{c}_i\cdot\mathbf{u})^2 - \frac{1}{48c^2}\mathbf{u}^2\right). \tag{5}$$

The corresponding mass density is $\rho=\Sigma_i f_i$ and the momentum density is $\rho\mathbf{u}=\Sigma_i f_i\mathbf{c}_i$. The pressure and kinematic viscosity are given in

$$p=\frac{3\rho c^2}{8}, \quad v=\frac{c^2\Delta t}{6}(2\tau-1). \tag{6}$$

For gaseous microflows, the relaxation parameter τ in the lattice Boltzmann equation with BGK collision approximation is modified to consider the gas compressibility[29]

$$\tau'=\frac{1}{2}+\frac{\rho_{\mathrm{ref}}}{\rho}\left(\tau-\frac{1}{2}\right), \tag{7}$$

where ρ_{ref} is the constant reference mass density.

Application of the multiscale technique (Chapman–Enskog expansion) yields the Navier–Stokes equation with dynamic viscosity

$$\eta=\frac{\rho_{\mathrm{ref}}c^2(\tau-0.5)\Delta t}{3}. \tag{8}$$

According to the knowledge of gas kinetic theory, the ratio of the mean-free path to the characteristic length, known as the Knudsen number, is determined by[33]

$$\mathrm{Kn}=\frac{\lambda}{H}=\frac{\eta\sqrt{\pi}}{H\sqrt{2\rho^2RT}}. \tag{9}$$

Since the Knudsen number changes along the microchannel and, in most cases, the outlet conditions are known (usually at atmospheric condition), the expression of the Knudsen number at the channel outlet determined by the outlet parameters (temperature and density) can be derived. After substituting Eq. (8) into Eq. (9), employing the equation of state for a perfect gas ($\rho=p/RT$) and Eq. (4), and neglecting the derivation process for simplicity, we obtain the final expression of the outlet Knudsen number as the following form for Qian's equilibrium function:

$$Kn_0=\sqrt{\frac{\pi}{24}}\frac{(2\tau-1)\rho_{\mathrm{ref}}}{\rho_0 N_y}. \tag{10}$$

Here, we assume uniform mesh ($\Delta x=\Delta y=\Delta z$) and isothermal flow. N_y, the number of lattice units in the y direction, satisfies $H=N_y\Delta y$. Likewise, employing Eq. (6), we can obtain the expression of the outlet Knudsen number dependent on the relaxation time for Grunau's equilibrium function

$$Kn_0=\sqrt{\frac{\pi}{27}}\frac{(2\tau_0-1)\rho_{\mathrm{ref}}}{\rho_0 N_H}. \tag{11}$$

In the lattice Boltzmann method, the bounce-back treatment ($f_8=f_{12}$ and $f_2=f_5$) schematic in Fig. 2 is usually applied at the solid wall to ensure a nonslip condition, and so is the specular reflection ($f_{10}=f_{12}$) for the slip boundary.[17] More generally, a surface is neither purely specular nor purely bounce-back. To accurately capture the slip velocity on the gas-solid wall, we combine the bounce-back treatment with the specular reflection in our simulation.[29] This boundary treatment is something like the diffuse reflection based on the molecules' collisions in gas kinetics. Lately, we also found that a similar combination of boundary condition was adopted in Ref. 34 to describe the phonons' interactions with the surface in a nanoduct.

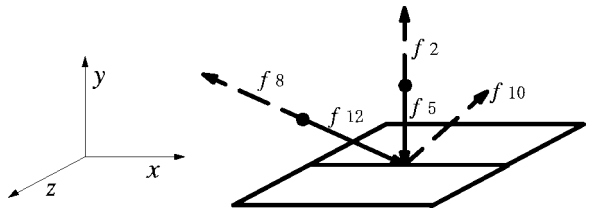

FIG. 2. The schematic of the boundary treatments.

With regard to the inlet and outlet boundaries, the pressure or density at the inlet and outlet are fixed, and velocity components are extrapolated from the downstream or upstream. Thus the five unknown distributions f_1, f_7, f_9, f_{10}, and f_{12} at the inlet and f_4, f_8, f_{11}, f_{13}, and f_{14} at the outlet can be obtained.

III. RESULTS AND DISCUSSION

A. 3D microducts flow

In the present computation, the height (y direction) of the simulated channel is fixed at $H=1.2$ μm and the length (x direction) is kept constant at $L=50$ H. The aspect ratio of the cross section, defined as the height to the width W (z direction), ranges from 0 (2D parallel plates) to 1 (square duct), assuming $H\leqslant W$ and the width is determined by the value of H/W in the simulation. The working fluids are carbon dioxide (CO_2), nitrogen (N_2), hydrogen (H_2), and helium (He). Their corresponding Knudsen numbers at the channel outlet Kn_0 are 0.0236, 0.055, 0.1, and 0.16, respectively. The $1000\times20\times20$ grid is used after the grid dependence test.

First, we compare the numerical results for employing the equilibrium function of Qian *et al.* with those for employing Grunau's equilibrium function. The outlet Knudsen number is $\mathrm{Kn}_0=0.055$, and the inlet-to-outlet pressure ratio is $P_i=p_i/p_0=1.94$. Aubert and Colin[35] proposed an analytical model for gaseous flows through rectangular microducts by solving the Navier–Stokes equation with second-order boundary conditions. Thus, the simulated results from the present LBM are also compared with the analytical data. The comparison is shown in Table I. We can see that the deviation is less than 3% between the LBM results and the analytical data, and the deviation is less than 1% between the simulated results from the equilibrium function of Qian *et al.* and Grunau's equilibrium function. This result shows that the present LBM model for microflows is convenient to implement for different equilibrium functions and is of fairly strong applicability. Consequently, Grunau's equilibrium function is adopted in the following simulations.

Figure 3 shows the velocity vector distribution in the streamwise direction for nitrogen at $P_i=1.94$ ($X=x/L, Y=y/H, Z=z/W$). Seen from this figure, as the flow proceeds towards the outlet (from $X=0$ to $X=1$), due to the compressibility effect, the velocity (including the slip velocity at the wall) increases with the decrease in pressure or density. As the aspect ratio decreases from $H/W=1$ [Fig. 3(a)] to H/W

TABLE I. Comparison of results by using the equilibrium function of Qian *et al.*, Grunau's equilibrium function and Aubert's analytical solutions ($Kn_0=0.055$, $P_i=2.64$).

	$H/W=1$			$H/W=0.5$		
Mass flow rate	Qian	Grunau	Aubert	Qian	Grunau	Aubert
$(10^{-11}$kg/s)	2.9	2.93	2.86	8.93	9.01	8.92
C_f Re	11.05	10.92		12.77	12.65	

$=0.25$ [Fig. 3(b)], we can also see that the velocity drops more sharply near the lateral walls (the planes of $Z=0$ and $Z=1$) and flattens more obviously near the center.

Figures 4 and 5 show the isolines of the velocity components. The u velocity (see Fig. 4) gets its maximum velocity at the outlet ($X=0$ denotes the inlet and $X=1$ denotes the outlet). The v velocity (see Fig. 5) is negative in the upper-half channel ($Y>0.5$), while it is positive with the same magnitude in the lower-half channel ($Y<0.5$) and vanishes in the center plane of $Y=0.5$. The w-velocity distribution behaves similarly but vanishes in the center plane of $Z=0.5$ (we do not show the w-velocity figures due to the space limitation). The isolines of the velocity get denser near the $Y=0$ and $Y=1$ walls as the width (W) of the channel increases.

The average pressure distribution across the channel is presented in Figs. 6 and 7 in the form of $P'=(p-p_{li})/p_0$, where the linear pressure p_{li} is calculated as $p_{li}=(p_i-p_0)x/L+p_0$. The nonlinearity increases with the increase in the inlet-to-outlet pressure ratio and with the decrease in outlet Knudsen number. In other words, the compressibility makes the pressure depart from linear while the rarefaction keeps the pressure distribution to be linear. The largest nonlinear pressure increases as the aspect ratio decreases from 1 to 0.25. The locations, where the peak deviation from the linear occurs, shift towards the channel outlet as the compressibility increases or the rarefaction decreases. For example, the locations are $X=0.557$, 0.566, 0.576, 0.586 for the four increasing pressure ratios in Fig. 6(a) and $X=0.572$, 0.557, 0.532, 0.483 for the four increasing outlet Knudsen numbers in Fig. 7. It can be seen that the variation trends of the curves and the locations of the peak deviations agree well with the analytical data of Ref. 35.

The mass flow rate per unit channel width is shown in Fig. 8 for nitrogen and helium flow. From the figure we can see that the agreement between the presented LBM results and the analytical data is quite good. The mass flow rate per unit width increases as the aspect ratio H/W decreases, which is evident especially for larger pressure ratios. The ratio for mass flow rate per unit width of the 3D channel to 2D channel is shown in Fig. 9. From the figure we can see that the gap between the 3D channel and 2D channel is the largest for nonslip flow ($Kn=0$), while the gap for the helium flow is the lowest, which implies that the slip velocity at the lateral walls, due to the rarefaction effect, decreases the lateral wall influence on the mass flow rate in rectangular channels.

The rarefaction effect on the flow-friction factor is shown in Fig. 10, where Reynolds number is defined based on the hydraulic diameter of the channel, $D_h=2WH/(W$

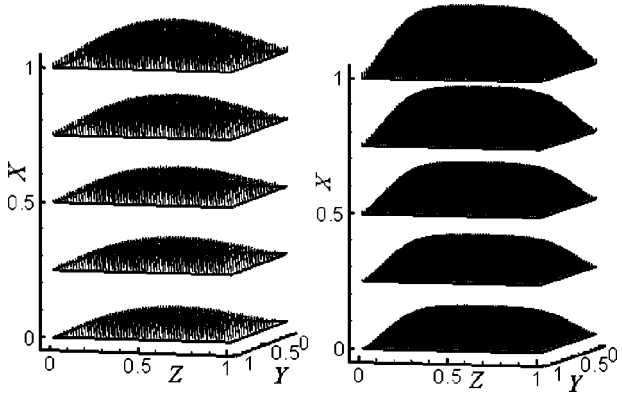

FIG. 3. Velocity vectors in the streamwise direction of the microchannel for nitrogen flow. (a) $P_i=1.94$, $H/W=1$; (b) $P_i=1.94$, $H/W=0.25$.

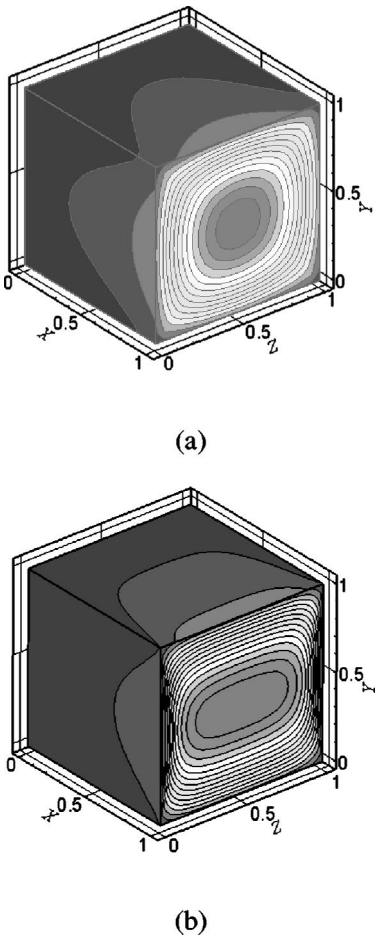

FIG. 4. The isolines of the u-component velocity for $P_i=1.94$ and $Kn_0=0.055$. (a) $H/W=1$; (b) $H/W=0.25$.

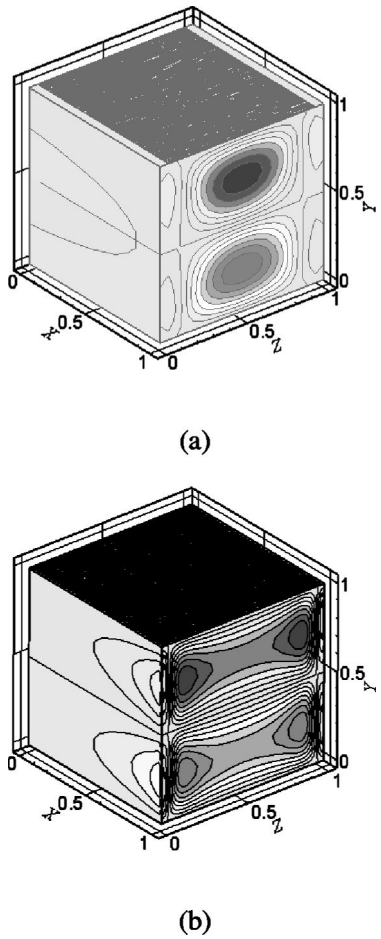

FIG. 5. The isolines of the v-component velocity distribution for $P_i=1.94$ and $\mathrm{Kn}_0=0.055$. (a) $H/W=1$; (b) $H/W=0.25$.

$+H$). The analytical solutions for the laminar, fully developed incompressible continuum flow provided by Shah and London[36] are adopted as the nonslip (Kn=0) results. From the figure we know that rarefaction decreases the flow resistance significantly. For the same Knudsen number, the friction factor increases as the aspect ratio decreases and reaches the maximum for a 2D parallel channel, which is in accordance with the behavior in the continuum flow. In addition, the shown average friction factor, calculated as $\int_0^L (C_f \mathrm{Re})dx/L$, increases with the increase in the inlet-to-outlet pressure ratio, which results from the compressibility effect.

B. 3D microscale porous media flow

We simulate flows in the three-dimensional porous structure schematic in Fig. 11. Thirty identical cubes with a dimension of 1.2 μm are included in the domain of $H=W=L=8.4$ μm. The whole domain is divided into $112\times112\times112$ cubic lattices in the x, y, and z directions.

Figure 12 shows the calculated results of the velocity vectors at $Z=0.5$ plane for the carbon dioxide flow and nitrogen flow. In Figs. 12(a) and 12(b), the length of the vectors stands for the magnitude of the velocity and the length is normalized with an equal scale for both figures. From the figure it is found that the fluid avoids the bodies and goes through open spaces. In addition, comparing Fig. 12(b) with

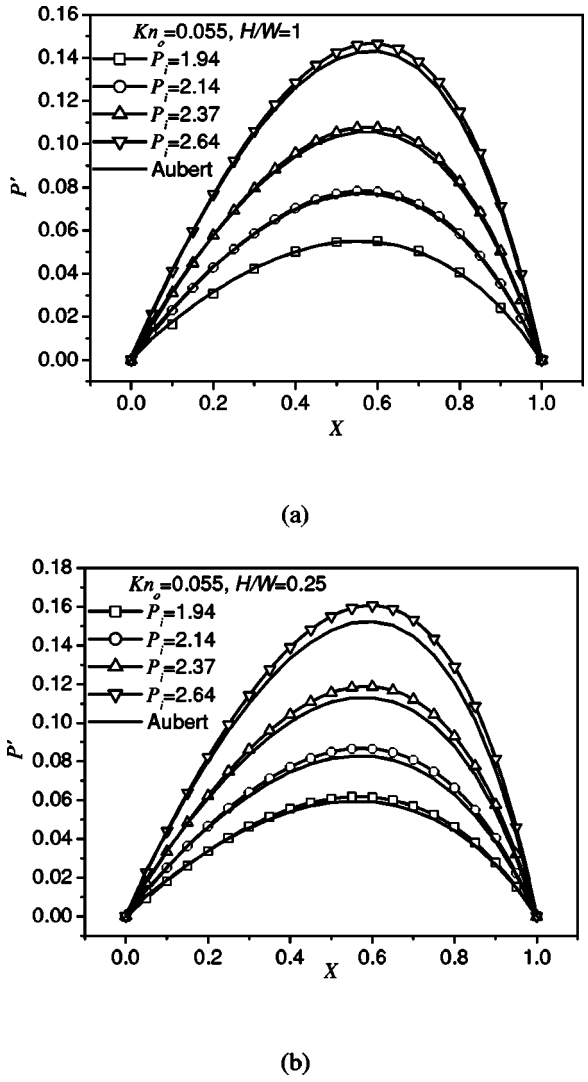

FIG. 6. Nonlinear pressure profiles for $\mathrm{Kn}_0=0.055$. (a) $H/W=1$; (b) $H/W=0.25$.

Fig. 12(a), we can see that the velocity near the bodies is increased while the velocity away from the bodies is decreased due to the larger rarefaction influence presented in Fig. 12(b), which is similar with the behavior that the normalized velocity distribution across the channel flattens in a 2D microchannel as the Knudsen number increases.[37]

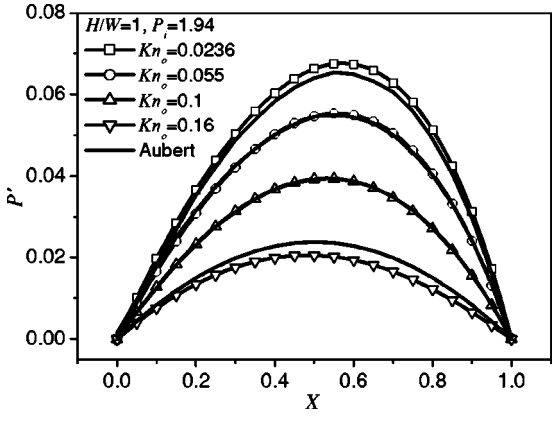

FIG. 7. Nonlinear pressure profiles for different Knudsen numbers.

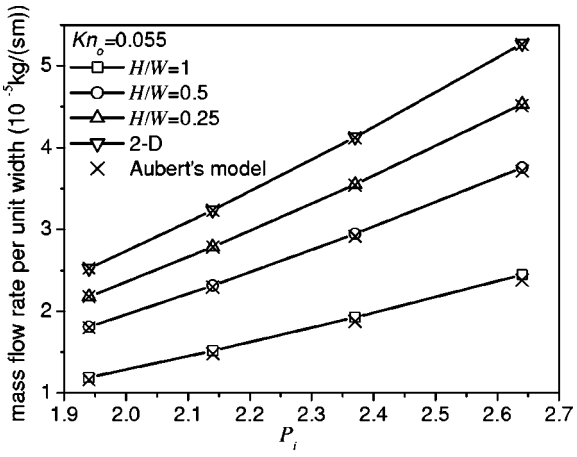

(a)

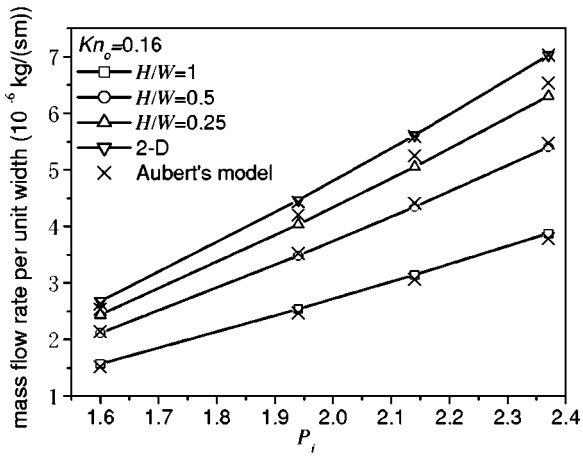

(b)

FIG. 8. Mass flow rate per unit channel width. (a) $Kn_0=0.055$; (b) $Kn_0=0.16$.

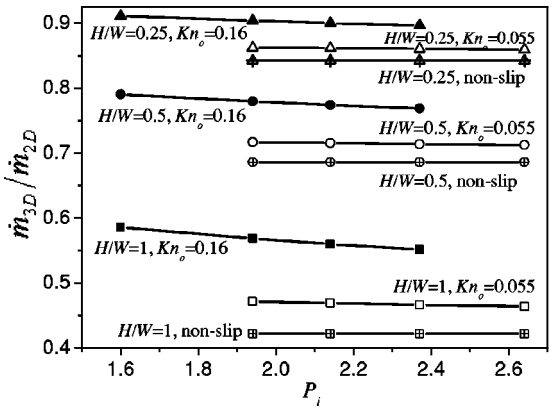

FIG. 9. Ratios for mass flow rate per unit width of 3D channel to 2D channel.

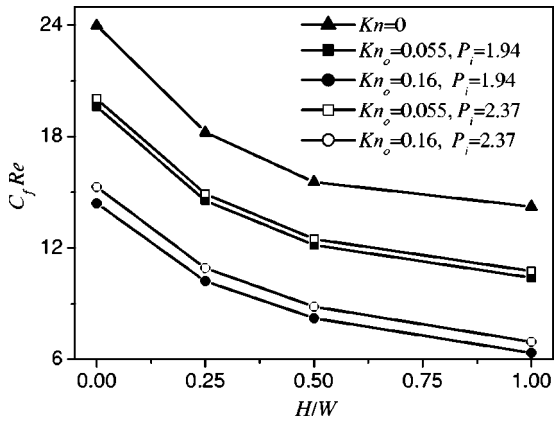

FIG. 10. Average friction factors in the channels as a function of aspect ratio.

Considering the gas-slip effect, Klinkenberg proposed the following gas permeability expression through a porous structure[38]

$$k_g = k_\infty\left(1+\frac{b}{\overline{p}}\right), \tag{12}$$

where $\overline{p}$ is the average pressure of the inlet and outlet and k_∞ is the absolute permeability, or permeability unaffected by the slip flow. To confirm the Klinkenberg equation, the simulated results are plotted as the relationship between the gas permeability and the inverse of the average pressure. The gas permeability is calculated from the pressure and flow data using a non-Klinkenberg gas-flow solution of compressible gas,[39]

$$k_g = \frac{2\eta L q_0 p_0}{p_i^2 - p_0^2}, \tag{13}$$

where p_i, p_0, and q_0 are inlet pressure, outlet pressure, and outlet velocity, respectively.

The comparison between the simulation results and experimental data[40] for gas permeability are shown in Fig. 13. The experimental results in Fig. 13(b) are scanned from Ref. 40 directly. Since the detailed tested porous structure in Ref. 40 is unknown to us, we can only compare the results qualitatively. On the whole, the agreement between the presented LBM solutions and experimental results are good. As the

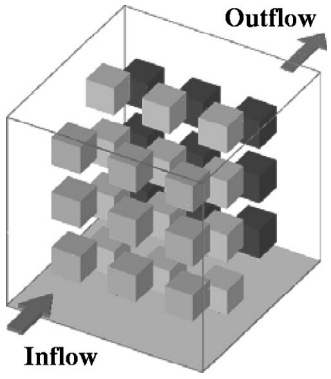

FIG. 11. A sketch of three-dimensional porous structure.

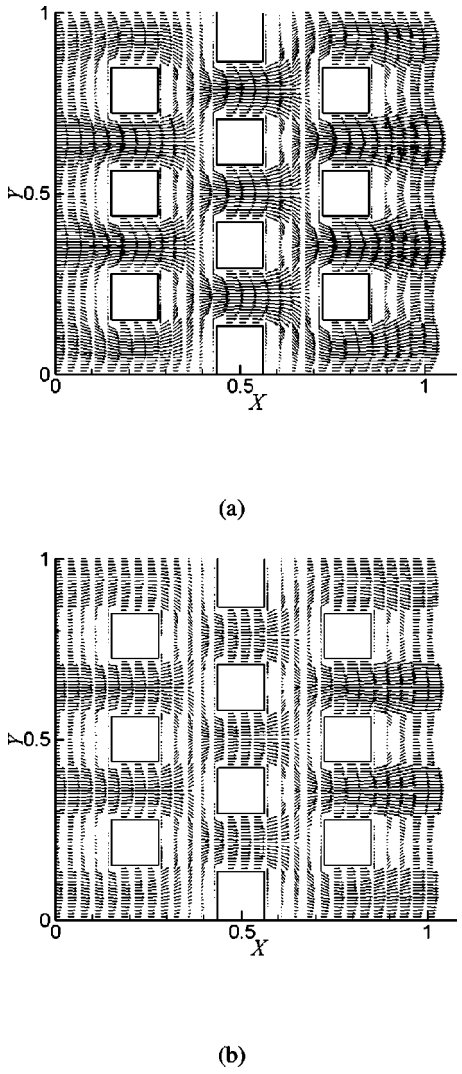

FIG. 12. Velocity vectors on the plane $Z=0.5$ in the porous structure. (a) Carbon dioxide flow, $P_i=1.5$ (Re=6.97). (b) Nitrogen flow, $P_i=1.5$ (Re =2.23).

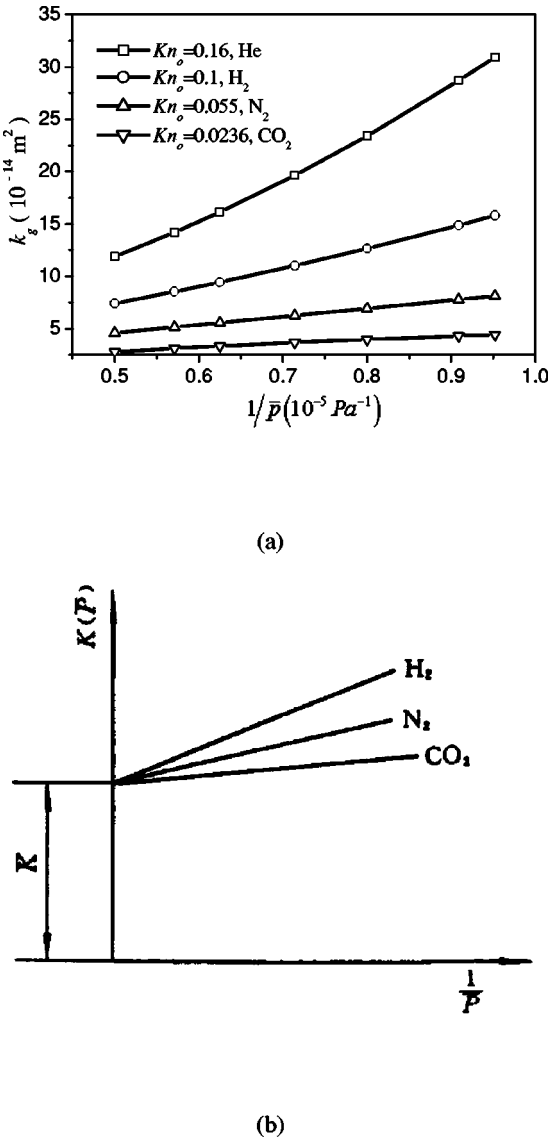

FIG. 13. Gas-permeability comparison of LBM results with experimental data. (a) The calculated gas permeability from the present LBM model. (b) The experimental results from Ref. 40.

Knudsen number increases, the rarefaction effect strengthens, and hence the gas permeability increases.

Also seen from Fig. 13(a), at relatively larger pressure ratios for higher Knudsen number (helium flow), the Reynolds number is relatively larger and the gas permeability profile shows a nonlinear behavior due to the inertial effects or nonlinear drag-force influence.

IV. CONCLUSIONS

In this paper, we have presented a three-dimensional lattice Boltzmann model for a gaseous flow in rectangular microducts. The combined effects of compressibility and rarefaction on gas microflows have been investigated with the model. A nonlinear pressure distribution is established in the microducts and the rarefaction negates the compressibility effect on the pressure profiles. The compressibility causes the curvature in the pressure distribution to be large and to shift towards the channel outlet while the rarefaction causes the curvature to be small and to shift towards the channel inlet. The curvature becomes larger as the height-to-width ratio (H/W) decreases. The velocity near the walls in the channel height direction increases evidently, and the corresponding velocity isolines get much denser as the aspect ratio decreases. The calculated mass flow rates fit analytical solutions quite nicely. In addition, the flow rate results show that the lateral wall influence on the flow rate in rectangular ducts is decreased due to the slip-velocity emergence at the walls.

Using the presented LBM model, the flow fields at a pore scale through 3D microscale porous structure are obtained for various pressure ratios and Knudsen numbers. The results show that gas permeability increases with the increase in rarefaction. The Klinkenberg equation is confirmed and the predicted gas permeability is consistent with the experimental results. In the lattice Boltzmann method, the bounce-back sheme means that when a particle reaches a wall node, the particle will scatter back to the fluid nodes along its incoming direction, while the specular reflection means the particle will reflect in the specular direction. This way of handling boundary conditions has been verified to be very simple compared with other numerical shemes.[17] It is still

convenient to extend the present boundary scheme by combining the bounce-back treatment with specular reflection to complicated geometries. Consequently, the present study indicates that the lattice Boltzmann method may be developed to be a high-efficient tool to simulate microflows due to its easier boundary treatments and higher computation efficiency compared to the DSMC or other numerical methods.

ACKNOWLEDGMENTS

This work was supported by the National Natural Science Foundation of China (Projects No. 50406020 and No. 50425620) and the National Key Project of Fundamental R&D of China (Project No. G2000026303).

[1]M. Gad-el-Hak, J. Fluids Eng. **121**, 5 (1999).
[2]P. Y. Wu and W. A. Little, Cryogenics **23**, 273 (1983).
[3]G. M. Mala and D. Q. Li, Int. J. Heat Fluid Flow **20**, 142 (1999).
[4]W. L. Qu, G. M. Mala, and D. Q. Li, Int. J. Heat Mass Transfer **43**, 353 (2000).
[5]D. Brutin and L. Tadrist, Phys. Fluids **15**, 653 (2003).
[6]E. B. Arkilic, M. A. Schmidt, and K. S. Breuer, J. Microelectromech. Syst. **6**, 167 (1997).
[7]J. C. Harley, Y. F. Huang, H. H. Bau, and J. Zemel, J. Fluid Mech. **284**, 257 (1995).
[8]A. Beskok, G. E. Karniadakis, and W. Trimmer, ASME J. Fluids Eng. **118**, 448 (1996).
[9]C. S. Chen, S. M. Lee, and J. D. Sheu, Numer. Heat Transfer, Part A **33**, 749 (1998).
[10]S. Roy and A. J. Baker, Numer. Heat Transfer, Part B **33**, 5 (1998).
[11]H. Xue, H. M. Ji, and C. Shu, Int. J. Heat Mass Transfer **44**, 4139 (2001).
[12]J. Koplik and J. R. Banavar, Annu. Rev. Fluid Mech. **27**, 257 (1995).
[13]G. A. Bird, *Molecular Gas Dynamics and the Direct Simulation of Gas Flows* (Clarendon, Oxford, 1994).
[14]T. Ohwada, Y. Sone, and K. Aoki, Phys. Fluids A **1**, 2042 (1989).
[15]S. K. Loyalka and S. A. Hamoodi, Phys. Fluids A **2**, 2061 (1990).
[16]S. Succi, *Lattice Boltzmann Equation for Fluid Dynamics and Beyond* (Clarendon, Oxford, 2001).
[17]S. Y. Chen and G. D. Doolen, Annu. Rev. Fluid Mech. **30**, 329 (1998).
[18]K. Balasubramanian, F. Hayot, and W. F. Saam, Phys. Rev. A **36**, 2248 (1987).
[19]D. H. Rothman, Geophysics **53**, 509 (1988).
[20]S. Succi, R. Benzi, and H. Francisco, Physica D **47**, 219 (1991).
[21]A. Adrover and M. Giona, Chem. Eng. J. **64**, 7 (1996).
[22]A. Koponen, M. Kataja, J. Timonen, and D. Kandhai, Int. J. Mod. Phys. C **9**, 1505 (1998).
[23]T. Inamuro, M. Yoshino, and F. Ogino, Int. J. Numer. Methods Fluids **29**, 737 (1999).
[24]M. Singh and K. K. Mohanty, Chem. Eng. Sci. **55**, 5393 (2000).
[25]J. Kim, J. Lee, and K. C. Lee, Physica A **293**, 13 (2001).
[26]Z. L. Guo and T. S. Zhao, Phys. Rev. E **66**, 036304 (2002).
[27]G. McNamara and G. Zanetti, Phys. Rev. Lett. **61**, 2332 (1988).
[28]S. Roy, R. Raju, H. F. Chuang, B. A. Cruden, and M. Meyyappan, J. Appl. Phys. **93**, 4870 (2003).
[29]G. H. Tang, W. Q. Tao, and Y. L. He, Int. J. Mod. Phys. C **15**, 335 (2004).
[30]S. Y. Chen, H. D. Chen, D. Martinez, and W. H. Matthaeus, Phys. Rev. Lett. **67**, 3776 (1991).
[31]Y. H. Qian, D. d'Humieres, and P. Lallemand, Europhys. Lett. **17**, 479 (1992).
[32]D. W. Grunau, Ph.D. thesis, Colorado State University, Fort Collins, 1993.
[33]S. A. Schaff and P. L. Chabre, *Flow of Rarefied Gases* (Princeton University Press, Princeton, NJ, 1961).
[34]W. S. Jiaung and J. R. Ho, J. Appl. Phys. **95**, 958 (2004).
[35]C. Aubert and S. Colin, Microscale Thermophys. Eng. **5**, 41 (2001).
[36]R. K. Shah and A. L. London, *Advances in Heat Transfer* (Academic, New York, 1978), Suppl. 1.
[37]G. E. Karniadakis and A. Beskok, *Micro Flows: Fundamentals and Simulation* (Springer, New York, 2001).
[38]L. J. Klinkenberg, *The Permeability of Porous Media to Liquids and Gases* (American Petroleum Inst., Drilling and Productions Practices, New York, 1941).
[39]A. E. Scheidrgger, *The Physics of Flow through Porous Media*, 3rd ed. (University of Toronto Press, Toronto, 1972).
[40]J. L. Ge, *Porous Flow Mechanics in Gas and Oil Reservoir* (Petroleum Industry Press, Beijing, 1982) (in Chinese).